Received: 26 July 2020 | Revised: 14 November 2020 | Accepted: 21 November 2020

DOI: 10.1002/ardp.202000241

FULL PAPER

ARCH PHARM DPhG
Archiv der Pharmazie

Synthesis, structural characterization, and biological studies of ATBS–M complexes (M(II) = Cu, Co, Ni, and Mn): Access for promising antibiotics and anticancer agents

Mohamed Ismael[1] | Laila H. Abdel-Rahman[1] | Doaa Abou El-ezz[2] | Ebtehal A.-H. Ahmed[1] | Ayman Nafady[3]

[1]Chemistry Department, Faculty of Science, Sohag University, Sohag, Egypt

[2]Department of Pharmacology and Toxicology, Faculty of Pharmacy, October University for Modern Sciences and Arts (MSA University), Giza, Egypt

[3]Department of Chemistry, College of Science, King Saud University, Riyadh, Saudi Arabia

Correspondence

Mohamed Ismael, Chemistry Department, Faculty of Science, Sohag University, Sohag 82524, Egypt.
Email: m_ismael@science.sohag.edu.eg

Ayman Nafady, Department of Chemistry, College of Science, King Saud University, Riyadh 11451, Saudi Arabia.
Email: anafady@ksu.edu.sa

Funding information

King Saud University, Grant/Award Number: RSP-2020/79

Abstract

A new bidentate Schiff base ligand (ATBS [4-bromo-2-(thiazole-2-yliminomethyl) phenol]) was synthesized via the condensation reaction of 2-aminothiazole with 5-bromosalicylaldehyde in ethanol. The reaction of ATBS with transition metal salts of Cu(II), Co(II), Ni(II), and Mn(II) afforded the corresponding ATBS–M complexes. Results from physicochemical and spectral analyses, such as elemental analysis, infrared, UV–Vis spectroscopy, magnetic susceptibility, and molar conductance, revealed a nonelectrolytic nature with octahedral (O_h) geometry and a metal/ligand ratio of 1:2 for Cu(II), Co(II), and Ni(II), but 1:1 for the Mn(II) complex. The density functional theory (DFT) calculations are correlated very well with the proposed structure and molecular geometry of the complexes as $[M(ATBS)_2]$ (M = Cu, Co, and Ni) and $[Mn(ATBS)(H_2O)_2]$. Significantly, the prepared compounds showed strong inhibition activity for a wide spectrum of bacteria (*Escherichia coli*, *Bacillus subtilis*, and *Staphylococcus aureus*) and fungi (*Candida albicans*, *Aspergillus flavus*, and *Trichophyton rubrum*), with the ATBS–Ni complex being the most promising antibiotic agent. Molecular docking studies of the binding interaction between the title complexes with the bacterial protein receptor CYP51 revealed clear insights about the inhibition nature against the studied microorganisms, with the following order: ATBS–Cu > ATBS–Mn > ATBS–Ni > ATBS–Co for complex stability. Moreover, the cytotoxicity measurements of all prepared metal complexes against the colon carcinoma (HCT-116) and hepatocellular carcinoma (Hep-G2) cell lines showed exceptional anticancer efficacy of the complexes as compared with the free ATBS Schiff base ligand. Significantly, the results attested that ATBS–Cu is the most effective complex against HCT-116 cells, whereas ATBS–Mn has the highest cytotoxic efficiency against Hep-G2 cells. Furthermore, electronic spectra, viscosity measurements, and gel electrophoresis techniques were employed to probe the interaction of all prepared ATBS–metal complexes with calf thymus (CT)-DNA. Results confirmed that all complexes are strongly bound to CT-DNA via intercalation mode, with the ATBS–Co complex having the highest binding ability.

KEYWORDS

antibiotics, anticancer, complexes, CT-DNA, DFT, molecular docking, thiazoles

1 | INTRODUCTION

Schiff bases are derived from the condensation of primary amines and aldehydes or ketones[1,2]; therefore, they are considered as "privileged ligands."[3] Moreover, they contain azomethine linkage, which plays a vital role in coordination with metal ions.[4] Schiff bases have a remarkable ability in stabilizing many different metals in various oxidation states[5]; thus, their complexes have gained considerable attention from most inorganic/materials researchers.[6] In this respect, Schiff base complexes have been extensively utilized in catalysis, organic synthesis, polymers stabilization, and dyes.[7] In particular, Schiff base complexes derived from salicylaldehydes with aromatic amines have received much attention, owing to the possible existence of nitrogen, oxygen, or sulfur as heteroatoms in their structure.[8]

Practically, the presence of heteroatoms in the structure of organic compounds enhances their biological activities. For instance, thiazoles as heterocyclic compounds have great importance as precursors for several organic compounds such as thiamine and penicillin, which is the most well-known antibiotic. Thus, the presence of heterocyclic compounds as thiazoles in the structure of Schiff bases markedly improved their medicinal and pharmaceutical applications[9] as antimicrobial, anti-inflammatory, anti-HIV agents, and anticancer drugs.[10]

DNA plays a very important role in a number of life processes, as it is the depot of hereditary information that governs cellular functions. Therefore, DNA is the main intracellular target of anticancer drugs that interact with it in different binding modes. Cu(II), Ni(II), Co(II), and Zn(II) Schiff base complexes showed interesting binding and cleavage activities with DNA.[11] Nowadays, researchers are focusing their efforts on developing effective therapeutic drugs for the treatment of chronic and incurable diseases. Consequently, we provide herein facile procedures for the synthesis of a novel Schiff base ligand derived from 2-aminothiazole and 5-bromosalicylaldehyde. Furthermore, this study is extended to develop a new class of Cu(II), Co(II), Ni(II), and Mn(II) Schiff base complexes as bioactive and selective compounds having promising antibiotics and anticancer activities. Additionally, the prepared complexes were characterized by several physicochemical and spectral techniques. Their DNA interaction, cytotoxicity, and antimicrobial activity were also studied. The final optimized geometries of the prepared compounds were established by employing the principles of the density functional theory (DFT) in addition to calculations of their universal chemical reactivity descriptors.

2 | RESULTS AND DISCUSSION

2.1 | Chemistry

2.1.1 | Structural interpretation

The Schiff base ligand ATBS (4-bromo-2-(thiazole-2-yliminomethyl) phenol) was prepared by mixing 2-aminothiazole with 5-bromosalicylaldehyde in a 1:1 molar ratio in absolute ethanol. The compounds were recrystallized from petroleum ether. The purity of ATBS Schiff base and its complexes was checked by thin-layer chromatography technique in the presence of methanol/chloroform as the eluent. The ATBS Schiff base ligand and its complexes were also characterized by microanalytical, physical, and spectral measurements (Table 1). The results of C, H, N, and S analyses for all complexes were in good agreement with the calculated values. Thus, it is clearly established that the Schiff base complexes exhibited a 1:2 metal-to-ligand ratio, except in the case of ATBS–Mn that favored a 1:1 molar ratio.

The qualitative characterization of the ATBS–Co and ATBS–Mn complexes for the identification of Cl^- ion was carried out by taking a small amount of the complex in a test tube. Then, concentrated nitric acid was added and the solution was heated up to the decomposition temperature of the complex. Next, silver nitrate was added to the mixture, which led to the formation of a white precipitate of silver chloride in the case of ATBS–Mn complex only, thereby confirming its presence in the structure of the complex.

2.1.2 | Infrared (IR) spectral studies

The IR spectral data of the ATBS Schiff base ligand and its metal complexes were determined with KBr in the range of 400–4000 cm^{-1} (Figure S1a–d). The IR spectrum of the ATBS Schiff base ligand showed the characteristic bands at 3409, 1627, and 1325 cm^{-1}, which were assigned to υ(OH), υ(C═N), azomethine group, and υ(C–O), respectively. Moreover, the Schiff base ligand showed a medium band at 758 cm^{-1}, attributed to υ(C–S) of the thiazole ring.[12] In addition, the Schiff base ligand exhibited a weak band at 3083 cm^{-1}, which is assigned to the aromatic ring vibration. The IR spectra of the prepared complexes were compared with that of the corresponding free ATBS Schiff base ligand to deduce the mode of chelation between the Schiff base ligand and the metal ion in the prepared complexes. The comparative spectra of the prepared Schiff base complexes revealed the disappearance of the band characteristic of the phenolic OH group, thereby indicating the deprotonation of the hydroxyl group of 5-bromosalicylaldehyde. This was also supported by the shift in υ(C–O), which appeared at 1305–1384 cm^{-1} upon complexation. The presence of a broad band at 3383–3419 cm^{-1} in the spectra of ATBS–Co, ATBS–Ni, and ATBS–Mn can be attributed to the OH of lattice water molecules.[13] This band disappeared in the spectrum of ATBS–Cu, implying that the structure of the complex does not contain any water molecules. More important, the corresponding Schiff base azomethine linkage appeared in the spectra of the prepared complexes at 1626–1651 cm^{-1}. The marked shift in the intensity of the azomethine linkage for some of the complexes confirmed the successful complexation between ATBS Schiff base ligand and the metal ions.[14] Finally, the weak IR bands appeared at 3000–3055 cm^{-1}, which are assigned to the aromatic CH.[15]

Furthermore, the spectra of the prepared ATBS–Cu, ATBS–Co, and ATBS–Ni Schiff complexes exhibited three new weak bands, assigned to υ(M–N), υ(M–O), and υ(M–S), as shown in Table 2. After complexation, a considerable shift occurred in the frequency of

TABLE 1 Physical and analytical data for ATBS Schiff base and its metal complexes

Compound	Empirical formula (M.W.), color	M.P. (°C)	Elemental analyses found (calc%)				Molar conduc. (μS)	μ_{eff} (μB)
			C	H	N	S		
ATBS	$C_{10}H_7N_2OSBr$ (283.15), light yellow	130	42.31 (42.38)	2.35 (2.47)	9.75 (9.88)	11.27 (11.30)	–	–
ATBS–Cu	$[C_{20}H_{14}N_4O_2S_2Br_2]Cu$ (627.80), olive	>300	38.13 (38.22)	2.27 (2.23)	8.87 (8.92)	9.98 (10.19)	6.16	2.07
ATBS–Co	$[C_{20}H_{18}N_4O_2S_2Br_2]Co$ (659.20), green	>300	36.50 (36.40)	2.65 (2.73)	8.53 (8.49)	9.75 (9.70)	24.3	2.65
ATBS–Ni	$[C_{20}H_{18}N_4O_4S_2Br_2]Ni$ (659.00), orange	>300	36.38 (36.41)	2.80 (2.73)	8.37 (8.49)	9.93 (9.71)	17.09	3.09
ATBS–Mn	$[C_{10}H_{12}N_2O_4SClBr]Mn$ (426.55), yellow	>300	28.11 (28.13)	2.78 (2.81)	6.59 (6.56)	7.46 (7.50)	15.03	5.42

Abbreviation: ATBS, 4-bromo-2-(thiazole-2-yliminomethyl)phenol.

the C–S band in all the prepared complexes, except in the case of the ATBS–Mn complex. This shift confirmed the involvement of the sulfur atom in the chelation with the metal ions.

2.1.3 | Nuclear magnetic resonance (NMR) spectra

The NMR spectra of the prepared Schiff base ligand was carried out in deuterated dimethyl sulfoxide (DMSO)-d_6, as shown in Figure S2a,b. The results of ^{1}H NMR confirmed the expected structure and showed the following signals: δ = 11.5 ppm (s, 1H, OH), 9.29 ppm (s, 1H, CH═N), and 6.98–8.04 ppm (m, 5H, aromatic CH). The recorded ^{13}C NMR spectra results were in good agreement with the proton NMR results, showing the multiplicity, and chemical shifts of carbon atoms are summarized as follows: 111.19 ppm (C–CH═N), the aromatic carbon (119.73, 120.48, 122.26, 137.31, and 143.08 ppm) and thiazole carbon atoms (159.60, 161.46, 171.34 ppm).

2.1.4 | Molar conductance

The results of the molar conductivity at a concentration of 10^{-3} M of the synthesized ATBS Schiff base complexes in dimethylformamide (DMF) indicated their nonelectrolyte nature and the absence of anions outside the coordination sphere,[16] as depicted in Table 1.

2.1.5 | Magnetic moment studies

Determination of the magnetic susceptibilities of ATBS Schiff base complexes was carried out at room temperature. The values of the effective magnetic moment (μ_{eff}) were determined by the data of diamagnetic corrections and Pascal's constants according to Equation (1), and the results are listed in Table 1. The value of μ_{eff} for ATBS–Cu was 2.07 μB, which suggested an octahedral geometry, whereas in the case of ATBS–Co, the magnetic measurements showed 2.65 μB value, which is sufficient for octahedral geometry. As for the ATBS–Ni complex, magnetic measurements revealed that the complex has a μ_{eff} value of 3.09 μB, which is compatible with the range of the expected octahedral geometry of Ni(II) complexes.[17,18] Furthermore, it has been found that the ATBS–Mn complex stabilizes in an octahedral structure with a value of 5.42 μB and ML stoichiometry.[19]

$$\mu_{eff} = 2.84\sqrt{(\chi_M T)^{0.5}}\ \text{B. M.} \quad (1)$$

where μ_{eff} is the effective magnetic moment (in Bohr Magneton, B.M.), T is the temperature (K), and χ_M is the molar magnetic susceptibility after correction.

2.1.6 | Molecular electronic spectra

The electronic spectra measurements are essential for determining the nature of the ligand field around the metal ion in addition to

TABLE 2 Infrared spectral bands (cm^{-1}) of the prepared Schiff base and its complexes

Compound	υ(OH)/(H_2O)	$\Upsilon(CH)_{aromatic}$	υ(CH=N)	υ(C–S)	υ(C–O)	υ(M–N)	υ(M–O)	υ(M–S)
ATBS	3409(w)	3083(w)	1627(s)	758(m)	1325(s)	–	–	–
ATBS–Cu	–	3055(w)	1628(s)	787(m)	1391(s)	440(w)	562(w)	435(w)
ATBS–Co	3419(b)	3020(w)	1626(s)	766(m)	1374(s)	451(w)	538(w)	425(w)
ATBS–Ni	3383(b)	3050(w)	1630(s)	766(m)	1384(s)	451(w)	539(w)	426(w)
ATBS–Mn	3386(b)	3000(w)	1651(s)	760(m)	1384(s)	450(w)	537(w)	

Abbreviations: ATBS, 4-bromo-2-(thiazole-2-yliminomethyl)phenol; b, broad; m, medium; s, strong; w, weak.

confirmation of the geometries of the prepared complexes, as shown in Figure S3. The molecular electronic spectra of the prepared ATBS Schiff base complexes were recorded in the range of 200–800 nm at room temperature. The spectrum of the free ATBS Schiff base showed two bands at 360 and 368 nm. The first band is assigned to intraligand transition and the second band is attributed for n→ π^*. The spectra of the prepared ATBS Schiff base complexes revealed the disappearance of the last band and the presence of another new band due to the donation of the nitrogen lone pair electrons of the Schiff base to the metal ion. The comparative molecular electronic spectra of the prepared Schiff base complexes showed a band in the range of 606–680 nm, which is clearly observed upon expansion and attributed to d–d transition (Table 3). The results of the electronic spectra, together with those of the effective magnetic moment values (2.07, 2.65, 3.09, and 5.42 B.M.), confirmed the octahedral geometry for the prepared ATBS–Cu, ATBS–Co, ATBS–Ni, and ATBS–Mn complexes, respectively.

2.1.7 | Estimation of the stoichiometry of the prepared complexes

For determining the stoichiometry of the prepared complexes, continuous variation and molar ratio methods were carried out, as illustrated in Figures 1 and S4. The results of both methods revealed that the prepared complexes favored a metal-to-ligand ratio of 1:2, except in the case of ATBS–Mn that exhibited a 1:1 ratio. In the case of the continuous variation method, the curves in Figure 1 showed a maximum absorbance at a mole fraction (X_{ligand}) = 0.65 for ATBS–Cu, ATBS–Co, and ATBS–Ni complexes, thereby indicating a 1:2 ratio. In contrast, the obtained results for ATBS–Mn revealed again a metal-to-ligand ratio of 1:1 at mole fraction X_{ligand} = 0.54.[20]

2.1.8 | Evaluation of the formation constant values of the prepared complexes

The continuous variation method is used as a tool for determining the formation constant (K_f) values of the prepared complexes spectrophotometrically according to Equations (2) and (3), as shown in Table 4.

$$K_f = \frac{A/A_m}{C(1 - A/A_m)^2} \text{ for the 1: 1complex,} \quad (2)$$

$$K_f = \frac{A/A_m}{4C2(1 - A/A_m)^3} \text{ for 1: 2 complexes,} \quad (3)$$

where A_m is the absorbance at the maximum formation of the complex, A is the arbitrarily chosen absorbance values on either side of the absorbance mountain col (pass), and C represents the initial concentration of the metal. The values of the formation constant (K_f) for the prepared ATBS complexes indicated that the complexes were relatively highly stable. The K_f values of the synthesized complexes increase in the following order: ATBS–Cu > ATBS–Co > ATBS–Mn > ATBS–Ni. Furthermore, the stability constant (pK) and Gibbs free energy (ΔG^*) values for the prepared complexes were calculated, and they are summarized in Table 4.

Moreover, all the prepared complexes exhibited a negative value of Gibbs free energy, which is consistent with a spontaneous and favorable reaction. The pH stability profiles of the prepared ATBS Schiff base complexes, presented in Figure 2, showed good stability

TABLE 3 Electronic absorption spectra results of the prepared ATBS Schiff base ligand and its complexes

Compound	λ_{max} (nm)	ε_{max} ($dm^3\ mol^{-1}\ cm$)	Assignment
ATBS	368	5320	Intraligand
	360	5360	n → π*
ATBS–Cu	664	1106	d–d
	424	23,787	LMCT
	392	19,090	LMCT
	369	13,954	n → π*
ATBS–Co	676	541	d–d
	608	321	d–d
	449	443	LMCT
	392	1160	n → π*
ATBS–Ni	364	17.4	d–d
	419	279	LMCT
	391	375	n → π*
ATBS–Mn	417	382	LMCT
	392	441	d–d

Abbreviations: ATBS, 4-bromo-2-(thiazole-2-yliminomethyl)phenol; LMCT, ligand-to-metal charge transfer.

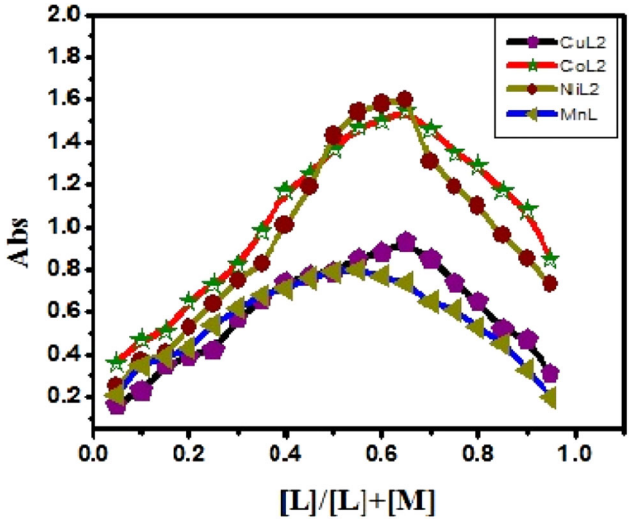

FIGURE 1 Continuous variation plots for ATBS Schiff base complexes when [ATBS–Cu] = [ATBS–Mn] = 1×10^{-3}, [ATBS–Co] = [ATBS–Ni] ≈ 10^{-2}, and at 298 K. ATBS, 4-bromo-2-(thiazole-2-yliminomethyl)phenol

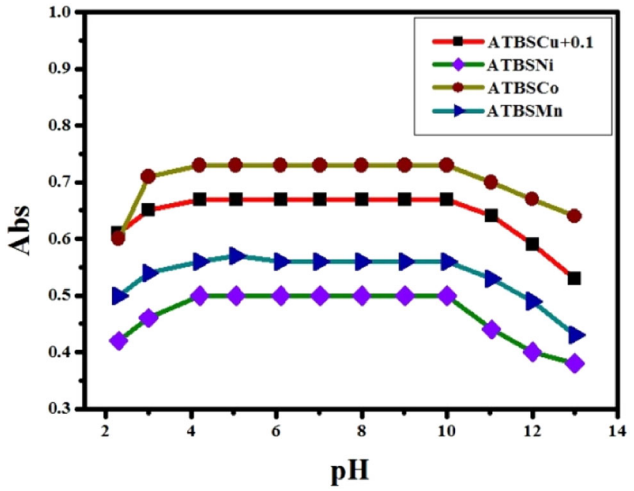

FIGURE 2 pH profiles for the prepared ATBS Schiff base complexes in DMF when [complex] = 10^{-3} M and at 298 K. ATBS, 4-bromo-2-(thiazole-2-yliminomethyl)phenol; DMF, dimethylformamide

over a wide pH range (3–9). From the obtained results, it is clearly established that the formation of the complex strongly enhanced the stability of the prepared Schiff base ligand. Consequently, the appropriate pH range for the different applications of the prepared ATBS Schiff base complexes is from 3 to 9.

2.1.9 | Theoretical study of ATBS Schiff base ligand and its complexes

The structural elucidation of the ATBS molecule was performed using DFT calculations to determine its 3D geometry and estimate the electronic descriptors. The ligand was found to be planar and had three coordination sites at hydroxyl, imino, and thiol groups (Figure 3a), and all of them were oriented toward each other. The molecular orbital (MO) calculations revealed that there was extensive charge distribution around the thiazole ring, imino, and hydroxyl groups, thereby indicating that chelation of the ligand around the metal ion takes place through these donor groups. The energy calculations of the highest occupied molecular orbital (HOMO) and the lowest unoccupied molecular orbital (LUMO) revealed that electron delocalization occurred all over the ATBS Schiff base ligand with an 8.36 eV energy gap, as illustrated in Figure 3b.

TABLE 4 The formation constant (K_f), stability constant (pK), and Gibbs free energy (ΔG^*) data of the prepared ATBS Schiff base complexes in DMF at 298 K

Complex	M:L ratio	K_f	pK	ΔG^* (kJ/mol)
ATBS–Cu	1:2	3.59×10^8	8.55	−43.78
ATBS–Co	1:2	8.65×10^5	5.93	30.34
ATBS–Ni	1:2	4.43×10^4	4.64	−23.74
ATBS–Mn	1:1	5.43×10^5	5.73	−29.32

Abbreviations: ATBS, 4-bromo-2-(thiazole-2-yliminomethyl)phenol; DMF, dimethylformamide.

The optimized complex structures of Cu(II), Co(II), and Ni(II) ions with the ATBS Schiff base ligand (Figure 4) showed that all the complexes had an octahedral geometry with an M:L ratio of 1:2, giving rise to the general formula of [M(ATBS)$_2$]. The higher stability of these structures was retained due to the protonation of the hydroxyl groups and the formation of aromatic rings between the metal ions and donor groups of the ATBS ligand. From the calculations, it was obvious that all complexes were electronically stable when comparing their energy gaps with that of the ATBS ligand. To reduce the steric effect, ATBS molecules were oriented in a perpendicular plane to each other around the metal ion. Selected bond lengths and angles of the coordination sphere are listed in Table S5.

In contrast, in the case of the Mn–ATBS complex, the ligand coordinated with the metal center via the phenolic oxygen and imino group only, forming a six-membered ring, whereas the thiol groups did not participate in the coordination, as shown in Figure 5 and Table S5. The octahedral geometry of the complex was achieved by three water molecules and an anion (Cl^- ion in this case), affording a molecular formula of [Mn(ATBS)(H_2O)$_3$Cl]. The stability of the optimized complexes was estimated by calculating the binding energy (BE), where the more negative BE corresponds to the most stable complex. According to the calculations, all complexes are more stable than their corresponding ligands with BE values of −405.81, −357.54, −286.84, and −316.66 for ATBS–Cu, ATBS–Co, ATBS–Ni, and ATBS–Mn, respectively.

To gain more information about the stability of the prepared Schiff base ligand and its metal complexes, the different global chemical descriptors were calculated according to relations (4–8), and the results are listed in Table 5. DFT calculations indicated that

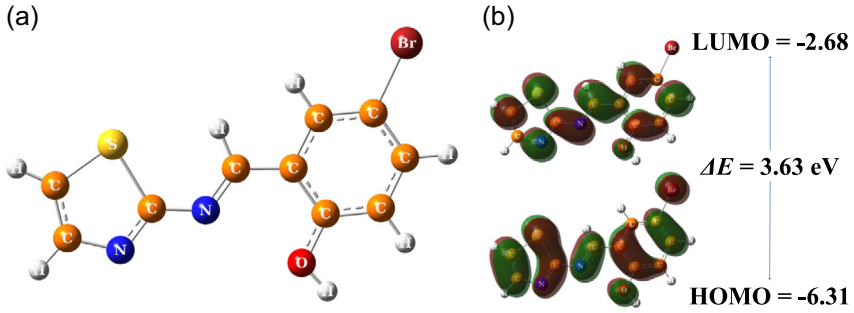

FIGURE 3 (a) Optimized structures of ATBS Schiff base ligand and (b) the HOMO–LUMO molecular orbitals with the calculated energy gap ΔE. ATBS, 4-bromo-2-(thiazole-2-yliminomethyl)phenol; HOMO, highest occupied molecular orbital; LUMO, lowest unoccupied molecular orbital

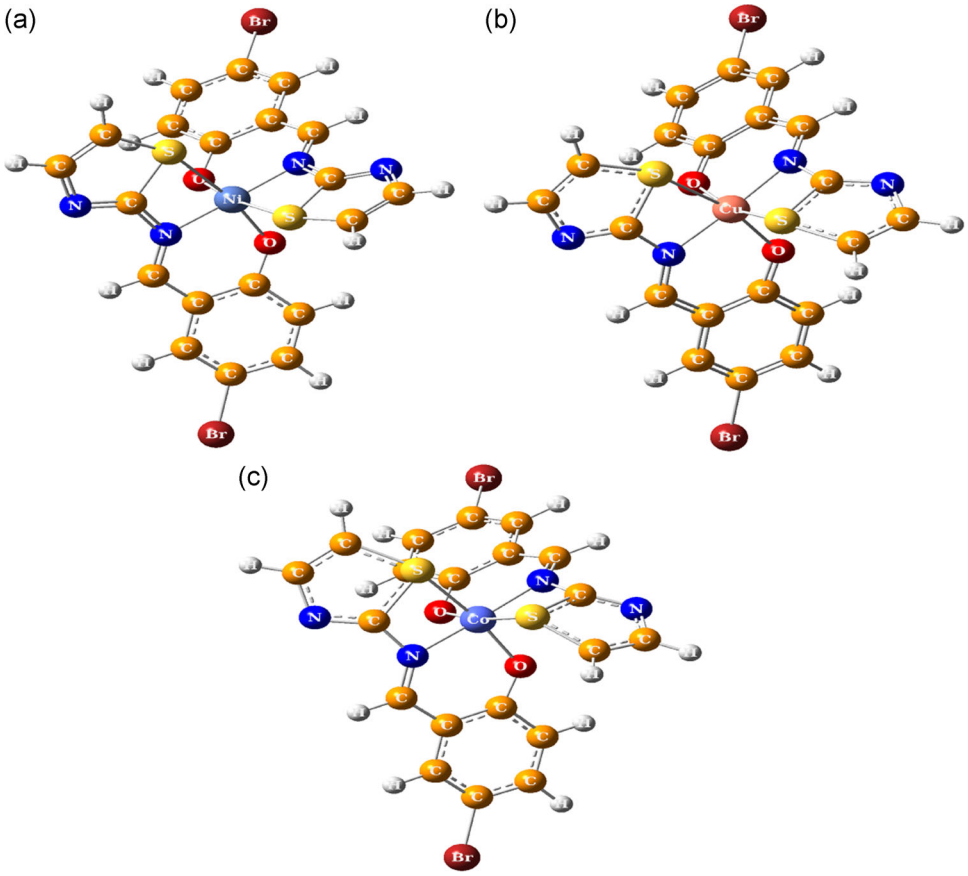

FIGURE 4 The optimized structures for (a) [Ni(ATBS)], (b) [Cu(ATBS)], and (c) [Co(ATBS)] complexes. ATBS, 4-bromo-2-(thiazole-2-yliminomethyl)phenol

all the prepared complexes are electronically active as compared with the ATBS ligand. This can be seen from both energy gap and chemical hardness descriptors:

$$\Delta E = E_{\text{LUMO}} - E_{\text{HOMO}}, \tag{4}$$

$$\eta = 1/2(E_{\text{LUMO}} - E_{\text{HOMO}}), \tag{5}$$

$$\chi = -1/2(E_{\text{LUMO}} + E_{\text{HOMO}}), \tag{6}$$

$$\mu = -\chi = 1/2(E_{\text{LUMO}} + E_{\text{HOMO}}), \tag{7}$$

$$\omega = \mu^2/2\eta. \tag{8}$$

where ΔE is the energy gap, η is the chemical hardness, χ is the electronegativity, μ is the chemical potential, and ω is the electrophilicity index.

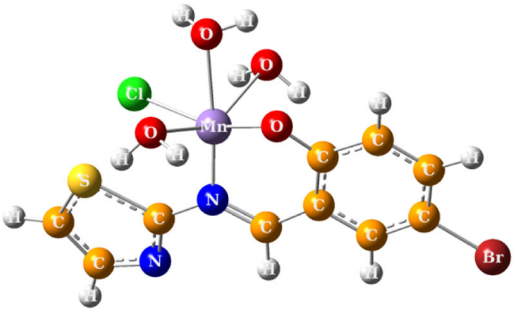

FIGURE 5 The optimized structure of $[Mn(ATBS)(H_2O)_3Cl]$. ATBS, 4-bromo-2-(thiazole-2-yliminomethyl)phenol

TABLE 5 The calculated global chemical reactivity descriptors of the prepared ATBS Schiff base and its complexes

Model	HOMO	LUMO	ΔE	η	μ	ω	χ
ATBS	−9.34	−0.98	8.36	4.18	−5.16	3.19	5.16
ATBS–Cu	−8.10	−1.78	6.32	3.16	−4.94	3.86	4.94
ATBS–Co	−7.11	−2.19	4.92	2.46	−4.65	4.40	4.65
ATBS–Ni	−8.31	−1.53	6.78	3.39	−4.92	3.57	4.92
ATBS–Mn	−7.84	−1.49	6.35	3.17	−4.66	3.43	4.66

Note: All values are expressed in eV unit.

Abbreviations: ATBS, 4-bromo-2-(thiazole-2-yliminomethyl)phenol; HOMO, highest occupied molecular orbital; LUMO, lowest unoccupied molecular orbital.

2.2 | Biological activities of ATBS and its complexes

The in vitro antimicrobial activity evaluation of the prepared Schiff base ligand and its metal complexes was carried out against selected pathogenic strains of Gram-negative bacteria *Escherichia coli*, and Gram-positive bacteria *Bacillus subtilis* and *Staphylococcus aureus* (Figure 6a), and three types of fungi, including *Candida albicans*, *Aspergillus flavus*, *and Trichophyton rubrum* (Figure 6b). All the investigated complexes revealed good inhibition results against the selected species. The comparative study of the prepared complexes with their respective ligand showed that the complexes have higher antimicrobial activity than the ligand, as summarized in Tables 6 and 7.

The antimicrobial activity of the prepared Schiff base complexes exhibits the following order: ATBS–Ni > ATBS–Cu > ATBS–Co > ATBS–Mn. These results can be demonstrated on the basis of the effect of the metal ions' nature, which affects the biological relevance upon coordination. Also, the geometry and steric effect play a vital role in facilitating the penetration of the target molecule into the cell of the microorganism.[21] Generally, Overtone's concept and chelation theory provided a comprehensive explanation for the higher antimicrobial activity of the metal complexes than their corresponding ligands. On chelation, the polarity of the metal ion will be reduced to a greater extent due to the overlap of the ligand orbital and partial sharing of the positive charge of the metal ion with donor groups. Furthermore, it increases the delocalization of π electrons over the whole chelating ring and enhances the penetration of the complexes into lipid membranes and blocking of the metal-binding sites in the enzymes of microorganisms. Solubility, conductivity, and bond length between the metal and ligand are remarkable factors that increase the activity.[22] Furthermore, the presence of the sulfur donor atom has a significant effect on the increase in the biological activity. This was evident from the higher activity values for ATBS–Ni, ATBS–Cu, and ATBS–Co complexes over the ATBS–Mn complex, which has the lowest one. For better understanding the effect of the prepared complexes on the growth of the selected microorganisms, the activity index was calculated for all the investigated compounds according to relation (9), and the results are listed in Table S1. The minimum inhibition concentration of the prepared compounds was estimated, and the obtained data were confirmed (Table 8). In view of the aforementioned results, it can be concluded that the prepared ATBS complexes may represent an important class of bioactive compounds, specially ATBS–Ni, which can be designed as a promising antibiotic agent.

2.3 | Molecular docking study

The protein substrate interaction plays a crucial role in the drug design process. Molecular docking was performed to understand the nature of interaction of the prepared compounds (ligand and complexes) with 14-alpha-demethylases of prominent fungal pathogen *C. albicans* (CYP51) enzyme. The crystal structure of CYP51 enzyme was used after removing all nonstandard moieties, and the active site

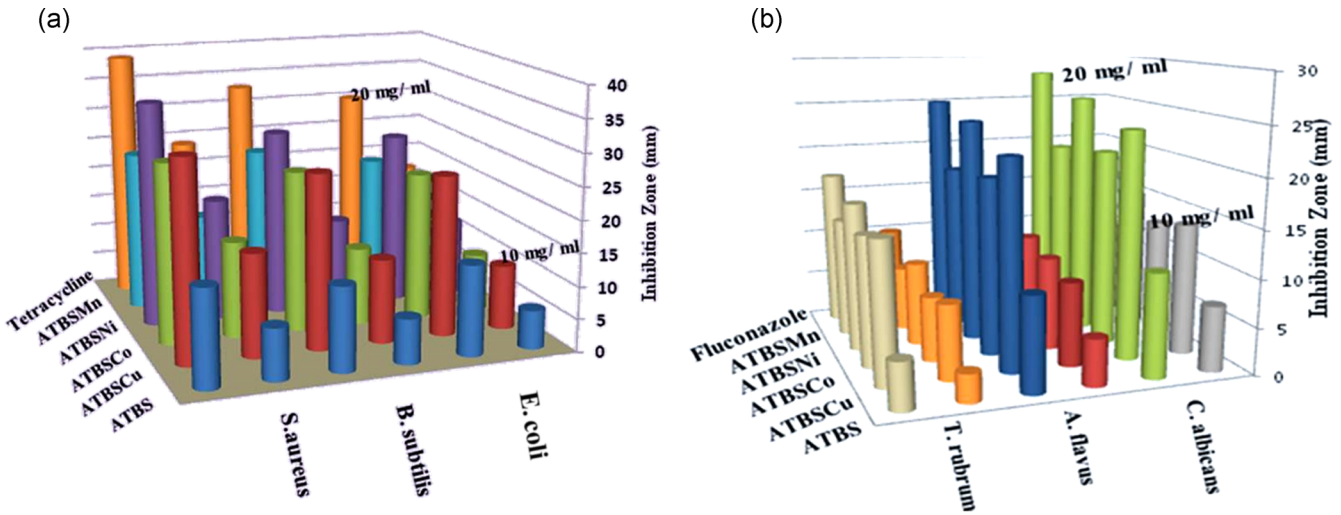

FIGURE 6 Histograms showing comparative (a) antibacterial and (b) antifungal activities of the prepared compounds

TABLE 6 Antibacterial activity results of the prepared ATBS Schiff base ligand and its complexes

Compound	Inhibition zone (mm)					
	Escherichia coli (−ve)		*Bacillus subtilis* (+ve)		*Staphylococcus aureus* (+ve)	
Conc. (mg/ml)	10	20	10	20	10	20
ATBS	6 ± 0.3	14 ± 0.5	7 ± 0.17	13 ± 0.25	8 ± 0.14	15 ± 0.16
ATBS–Cu	10 ± 0.11	25 ± 0.06	13 ± 0.27	27 ± 0.19	16 ± 0.12	31 ± 0.05
ATBS–Co	9 ± 0.13	23 ± 0.15	12 ± 0.07	25 ± 0.08	15 ± 0.11	28 ± 0.16
ATBS–Ni	12 ± 0.24	27 ± 0.17	14 ± 0.13	29 ± 0.14	19 ± 0.05	35 ± 0.09
ATBS–Mn	9 ± 0.16	21 ± 0.08	11 ± 0.06	24 ± 0.28	14 ± 0.09	25 ± 0.17
Tetracycline	17 ± 0.09	30 ± 0.22	16 ± 0.18	33 ± 0.15	24 ± 0.28	39 ± 0.06

Abbreviation: ATBS, 4-bromo-2-(thiazole-2-yliminomethyl)phenol.

TABLE 7 Antifungal activity results of the prepared ATBS Schiff base ligand and its complexes

Compound	Inhibition zone (mm)					
	Candida albicans		*Aspergillus flavus*		*Trichophyton rubrum*	
Conc. (mg/ml)	10	20	10	20	10	20
ATBS	7 ± 0.07	11 ± 0.07	5 ± 0.06	10 ± 0.25	3 ± 0.18	5 ± 0.06
ATBS–Cu	14 ± 0.24	24 ± 0.22	9 ± 0.24	22 ± 0.11	8 ± 0.30	15 ± 0.05
ATBS–Co	13 ± 0.16	21 ± 0.18	10 ± 0.11	19 ± 0.22	7 ± 0.19	14 ± 0.13
ATBS–Ni	15 ± 0.09	26 ± 0.30	11 ± 0.14	24 ± 0.17	9 ± 0.27	16 ± 0.16
ATBS–Mn	10 ± 0.23	20 ± 0.27	9 ± 0.23	18 ± 0.15	7 ± 0.10	13 ± 0.15
Tetracycline	16 ± 0.23	28 ± 0.17	12 ± 0.28	25 ± 0.08	10 ± 0.09	17 ± 0.23

Abbreviation: ATBS, 4-bromo-2-(thiazole-2-yliminomethyl)phenol.

was examined to determine the cavity size and hydrogen bond network. The active site pocket of the protein was found to be 5 Å in size, which was defined by four residues sets (62–92, 230–236, 374–377, and 498–513), as illustrated in Figure 7a. The residues in the active cavity had hydrophobic characters, which enabled their interaction with the nonaqueous substrates.[23]

Docked structures of the prepared compounds are shown in Figure 7b–f, and the calculated docking energies are listed in Table 9. Docking results showed that there is an interaction between all compounds and the active site of the enzyme. The main interaction forces included H-donor, H-acceptor, ionic, and π–H. The calculated energies of ATBS and its complexes indicated that the BE decreases upon coordination. These results suggested that complexation enhanced the biological activity of ATBS against the microbial cells. The order of the complexes' reactivity against CYP51 was as follows: ATBS–Cu > ATBS–Mn > ATBS–Ni > ATBS–Co.

TABLE 8 Minimum inhibition concentration (MIC; mg/ml) of ATBS Schiff base and its complexes against both bacteria and fungi

Compound	Minimum inhibition concentration					
	Bacteria			Fungi		
	Escherichia coli (−)	*Bacillus subtilis* (+)	*Staphylococcus aureus* (+)	*Candida albicans*	*Aspergillus flavus*	*Trichophyton rubrum*
ATBS	7.50	6.50	6.00	6.50	7.00	8.00
ATBS–Cu	3.00	2.00	1.50	2.00	3.50	4.00
ATBS–Co	3.50	2.50	2.00	3.50	3.00	4.30
ATBS–Ni	2.50	1.50	1.00	1.50	2.50	3.00
ATBS–Mn	4.00	3.00	3.50	4.50	4.00	5.00

Abbreviation: ATBS, 4-bromo-2-(thiazole-2-yliminomethyl)phenol.

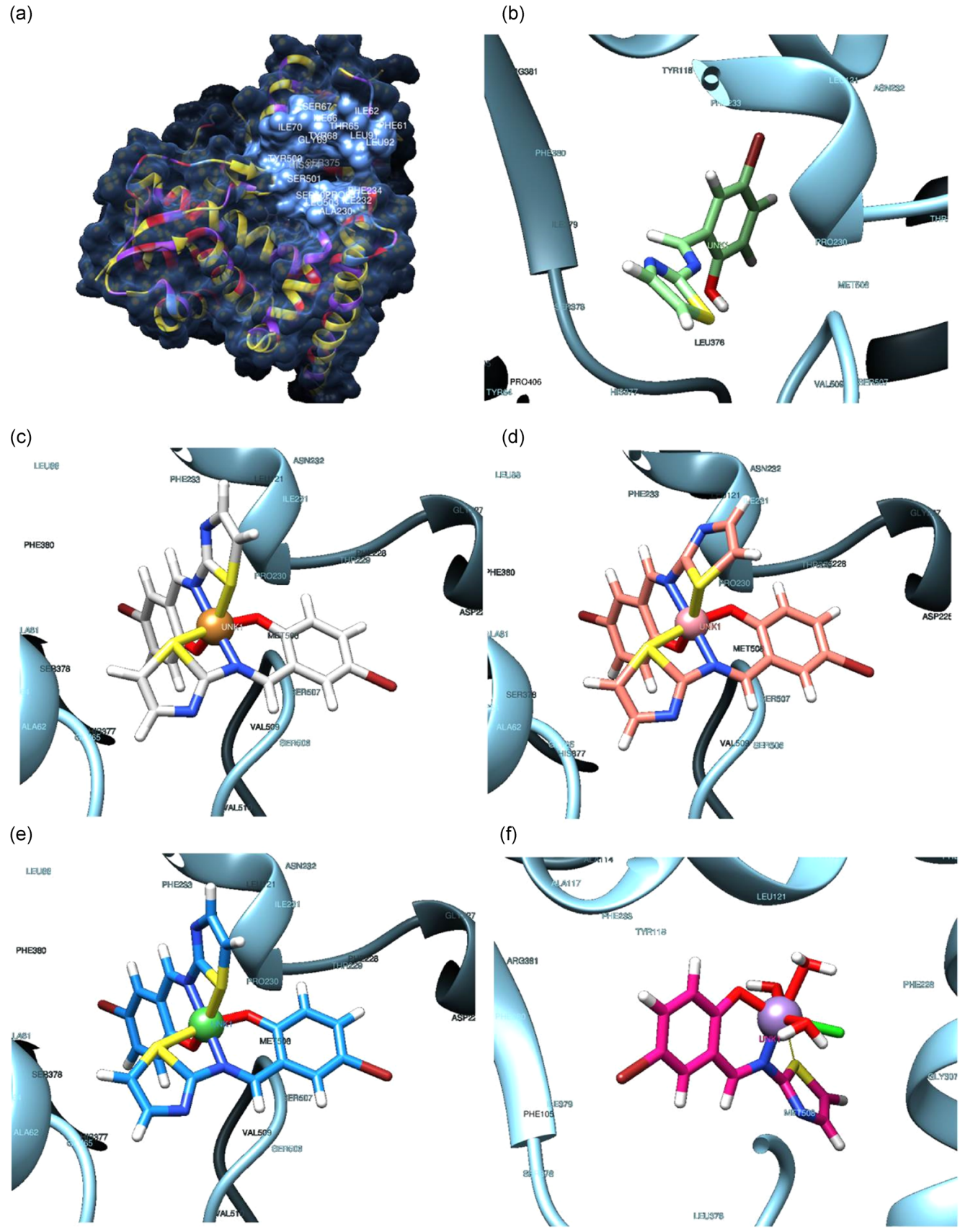

FIGURE 7 (a) The structure of the active site pocket of CYP51 protein and docking models of (b) ATBS (c) ATBS–Cu, (d) ATBS–Co, (e) ATBS–Ni, and (f) ATBS–Mn oriented in the active site. ATBS, 4-bromo-2-(thiazole-2-yliminomethyl)phenol

TABLE 9 Docking energy (DE) of the substrate models in the active pocket of CYP51 protein of the pathogen *Candida albicans*, with the donor/acceptor hydrogen bond formed with the surrounding residues

Model	DE (kJ/mol)	Donor	Acceptor	D-A (distance)
ATBS	−34.778526	HIS374	ATBS_S	4.202
		SER375	ATBS_N	4.305
		HIS377	ATBS_S	4.247
ATBS–Cu	−37.483765	GLN66	ATBS_N	4.354
ATBS–Co	−35.449785	HIS374	ATBS_S	4.202
		HIS377	ATBS_S	4.247
ATBS–Ni	−36.686581	GLN66	ATBS_N	4.354
ATBS–Mn	−37.483902	VAL509	ATBS_S	4.149

Abbreviation: ATBS, 4-bromo-2-(thiazole-2-yliminomethyl)phenol.

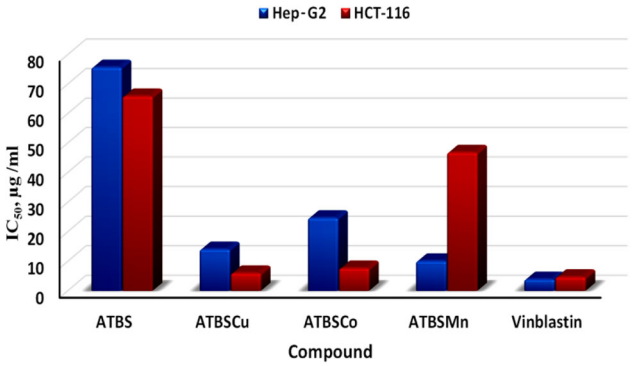

FIGURE 8 The anticancer activity, IC_{50} (μg/ml), of the ATBS Schiff base and its complexes against the human liver carcinoma cell line Hep-G2 and the human colon carcinoma cell line HCT-116, compared with the standard drug vinblastin. ATBS, 4-bromo-2-(thiazole-2-yliminomethyl)phenol

2.4 | Anticancer activity study

The cytotoxicity of the ATBS Schiff base and its Cu(II), Co(II), and Mn(II) complexes was estimated against two cancer cell lines, colon carcinoma (HCT-116) and hepatocellular carcinoma (Hep-G2) cell lines, and compared with the standard drug vinblastin, as depicted in Figure 8. It is obvious from the obtained results and the recorded values of IC_{50} that all the complexes displayed a significant cytotoxicity against both cancer cell lines. Moreover, the tested complexes were found to be more effective than their respective Schiff base ligand. Also, it is clear that ATBS–Cu is more effective against the colon carcinoma cell line, but ATBS–Mn has the highest value of cytotoxicity against hepatocellular carcinoma, as shown in Table S7.

2.5 | DNA binding studies

2.5.1 | Electronic absorption spectra

The mode and strength of interaction of the prepared ATBS Schiff base complexes with calf thymus DNA (CT-DNA) were probed by various spectral and analytical methods. The analysis of the absorption spectra of the prepared complexes upon the addition of CT-DNA is one of the most precise techniques used to estabilsh the binding with DNA. The binding ability of ATBS–Cu and ATBS–Co has been studied by UV–Vis spectroscopy with fixing the concentration of the prepared complex and varying the concentration of CT-DNA over the range of 30–150 μM. As the concentration of CT-DNA increases, the investigated ATBS Schiff base complexes showed a hypochromicity effect with a small shift in the wavelength. The binding ability of both complexes has been determined by calculating the value of the binding constant from relation (2) that has been previously mentioned in Section 2.1.8. The results revealed that ATBS–Co has the highest binding ability with CT-DNA with an intrinsic binding constant value equal to 1.23×10^4. Moreover, the results revealed that the investigated complexes exhibited an intimate interaction with CT-DNA. All the obtained data of DNA interaction with the prepared ATBS–Cu and ATBS–Co are described in Figure 9, and their binding constants are presented in Table S8 and Figure S9.

2.5.2 | Viscosity measurements as a methodology for DNA binding

The relative viscosity of CT-DNA was studied upon a gradual increase of the concentration of the prepared complexes, as shown in Figure 10. At the lower concentrations of the investigated complexes, there is a slight increase in the relative viscosity of DNA. It has been found that, as the concentration of the complex increases, a significant increase has been observed, but lower than those observed for the typical ethidium bromide (EB) intercalator. This behavior implied that the investigated complexes bind with CT-DNA via the intercalation mode. The observed increase in the viscosity measurements can be attributed to the increase in the DNA molecular length due to the insertion of the aromatic rings of the ligand into the DNA base pairs, which is expected to cause bending in the DNA helix.[24]

2.5.3 | Agarose gel electrophoresis

Agarose gel electrophoresis is an important methodology used for monitoring the binding of the investigated complexes with CT-DNA. The DNA cleavage of the investigated ATBS Schiff base complexes was studied using the gel electrophoresis method. It is obvious that, as the complexes cleave the DNA, therefore, they potentially inhibit the growth of pathogenic organism by cleaving the genome.[25] Moreover, the investigated complexes were found to have variable

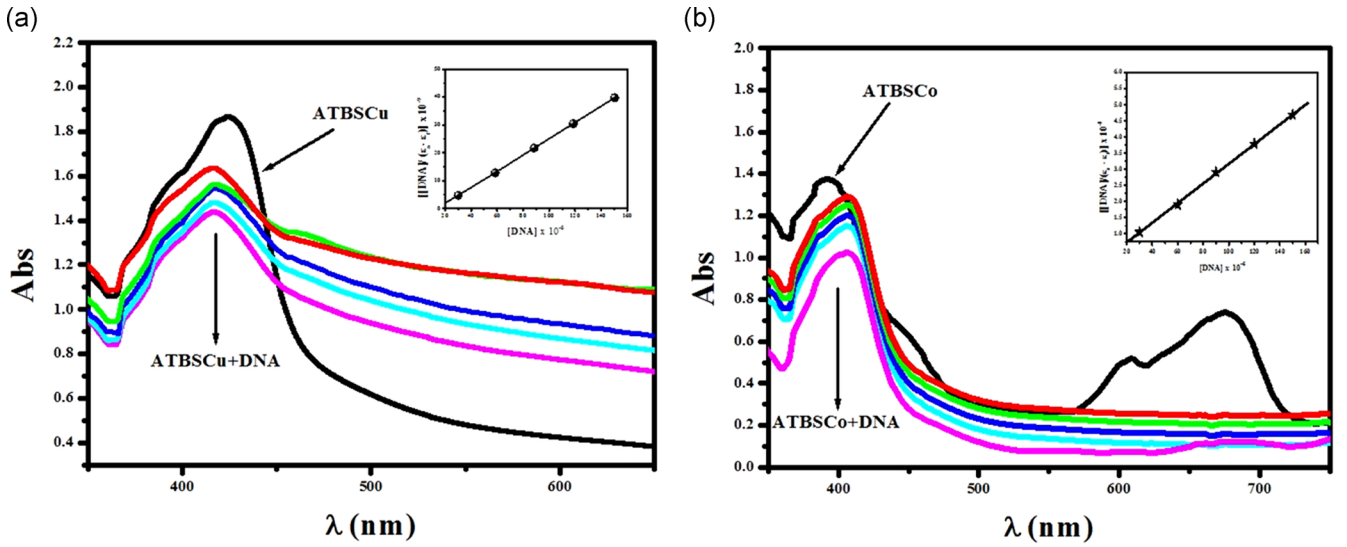

FIGURE 9 Absorption spectra of (a) ATBS–Cu (6.6×10^{-5} mol dm^{-3}) and (b) ATBS–Co (1×10^{-3} mol dm^{-3}) complexes in 0.01mol dm^{-3} Tris buffer (pH 7.2, 298 K) with CT-DNA (30–150 μM) from top to bottom. Inset: Plot of [DNA]/($\varepsilon_a - \varepsilon_f$) versus [DNA]. ATBS, 4-bromo-2-(thiazole-2-yliminomethyl)phenol; CT-DNA, calf thymus DNA

degrees of DNA cleavage as compared with the DNA ladder shown in Figure 11.

3 | CONCLUSION

In this study, a series of Cu(II), Co(II), Ni(II), and Mn(II) complexes with ATBS ligand was synthesized and characterized using elemental, spectroscopic, and theoretical methods. The prepared complexes were tested as antimicrobial agents, where they showed a high activity against *E. coli* and Gram-positive bacteria such as *B. subtilis* and *S. aureus*, as well as *C. albicans*, *A. flavus*, *and T. rubrum* fungal cells. Moreover, the anticancer activity of the prepared compounds was probed by studying their interaction with DNA of colon carcinoma (HCT-116) and hepatocellular carcinoma (Hep-G2) cell lines. Computational studies using DFT calculations and molecular docking studies were used to deduce the electronic structure of the complexes and evaluate the chemical descriptors responsible for the chemical activity and the binding modes with the protein receptors of the microorganisms. The obtained data implied that ATBS–Co has

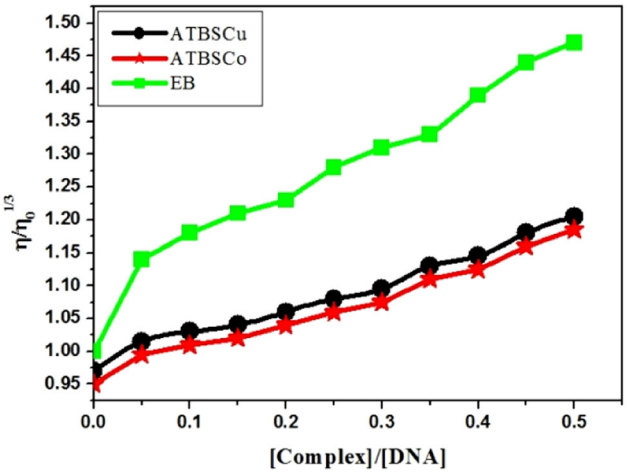

FIGURE 10 The effect of increasing the amount of ATBS–Cu and ATBS–Co complexes on the relative viscosity of CT-DNA when [DNA] = 0.5 mM [complex] and [EB] = 25–250 μM at 298 K. ATBS, 4-bromo-2-(thiazole-2-yliminomethyl)phenol; CT-DNA, calf thymus DNA; EB, ethidium bromide

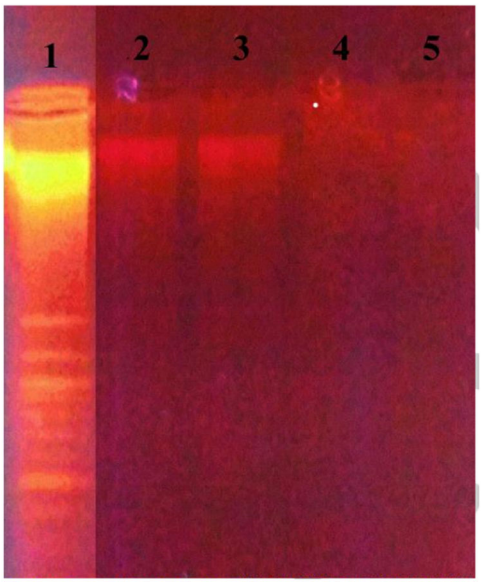

FIGURE 11 DNA binding results of the prepared Schiff base complexes based on gel electrophoresis. Lane 1, DNA ladder; Lane 2, ATBS–Cu + DNA; Lane 3, ATBS–Co + DNA; Lane 4, ATBS–Co; Lane 5, ATBS–Cu. ATBS, 4-bromo-2-(thiazole-2-yliminomethyl)phenol

the highest binding ability with CT-DNA with an intrinsic binding constant value equal to 1.23×10^4.

4 | EXPERIMENTAL

4.1 | Chemistry

4.1.1 | Materials and instruments

All chemicals used in this study such as transition metal salts [$Cu(CH_3COOH)_2{\cdot}H_2O$, $CoCl_2{\cdot}6H_2O$, $Ni(NO_3)_2{\cdot}6H_2O$, and $MnCl_2{\cdot}4H_2O$] and solvents were of reagent grade and used as received without further purification. Organic compounds such as 5-bromosalicylaldehyde and 2-aminothiazole were purchased from Merck Company. CT-DNA and tris(hydroxymethyl)aminomethane (Tris) were purchased from Sigma-Aldrich Chemie. Melting points and decomposition temperature of the synthesized Schiff base ligand and its complexes, respectively, were recorded on a Gallenkamp (UK) apparatus. The IR spectral data in the range of 400–4000 cm^{-1} were recorded on FTIR Alpha Bruker at the micro-analysis unit in Sohag University, using platinum ATR with KBr pellets. The PerkinElmer Model 240C Elemental Analyzer at the main lab of Cairo University was used for elemental analysis (C, H, and N). Bruker ARX 400 was the system used for NMR analysis of the ligand in deuterated *N*,*N*′-dimethyl sulfoxide (DMSO-d_6). The conductivity measurements of the synthesized metal complexes in DMF (10^{-3} M) at room temperature were carried out using Jenway conductivity/TDS Meter Model 4510. Magnetic susceptibility measurements were determined on Gouy's balance apparatus and $Hg[Co(SCN)_4]$ as a calibrant, and the calculated data of diamagnetic corrections were determined by Pascal's constants. UV–Vis spectra were recorded in DMF using 10-mm matched quartz on PG spectrophotometer model T80+. The absorbance of 1×10^{-3} M of the prepared complexes was determined at various pH levels. Antimicrobial screening of ATBS Schiff base complexes was carried out using the disc diffusion method in the Botany Department, Faculty of Science, Assuit University. The cytotoxicity was performed against cell lines colon carcinoma (HCT-116 cell line) and hepatocellular carcinoma (Hep-G2 cell line) at the National Cancer Institute, Cancer Biology Department, Pharmacology Department, Cairo University, using the sulforhodamine B stain (SRB) technique. Viscosity measurements were performed using an Ostwald viscometer immersed in a thermostated water bath at 25°C. Gel electrophoresis experiments were visualized under a UV transilluminator and photographed with a Panasonic DMC-LZ5 Lumix digital camera.

4.1.2 | General procedure for the synthesis of the ATBS Schiff base ligand

Here, 3 mmol (0.300 g) of 2-aminothiazole was mixed with 3 mmol of 5-bromosalcilaldehyde (0.603 g) in 20 ml ethanol for 1 h with continuous stirring at 70°C, followed by the addition of drops of piperidine as catalyst.[26] The reaction mixture was then stirred in ice for 2 h, and the yellow precipitate was filtered off, washed with ethanol, dried in vacuo over anhydrous $CaCl_2$, and recrystallized from petroleum ether.

4.1.3 | Synthesis of the Schiff base metal complexes

The Schiff base metal complexes (Scheme 1) were synthesized by mixing 1 mmol of the Schiff base (0.283 g) with equimolar amounts of the desired metal salts $Cu(CH_3COO)_2{\cdot}H_2O$ (0.199 g), $CoCl_2{\cdot}H_2O{\cdot}6H_2O$ (0.237 g), $Ni(NO_3)_2{\cdot}6H_2O$ (0.290 g), and $MnCl_2{\cdot}4H_2O$ (0.197 g), separately in 20 ml ethanol. The mixture was refluxed for 3 h at 50°C. The precipitated solid was evaporated, filtered, washed with ethanol, and dried in vacuo over anhydrous $CaCl_2$.[27] Attempts to grow single crystals suitable for the X-ray crystallographic analysis of all metal complexes were unsuccessful.

4.2 | Molecular modeling study

4.2.1 | DFT calculations

Theoretical calculations for the ATBS Schiff base ligand and its complexes models were performed using Gaussian 03 package[28] by applying the DFT approximation method. Calculations were carried out using 6-31G(d,p)[29] basis set for ATBS atoms and LANL2DZ[30] basis set with effective core potential for metal ions. Geometry optimization was carried out to obtain the most stable structures, define orientation of the donor groups around the central metal, and identify the 3D coordination geometry. Moreover frontier MO occupation for HOMO and LUMO orbitals had been computed and used to calculate selected chemical descriptors used for chemical reactivity estimation. Optimized structures as well as frontier MOs were visualized using GaussView 3.0 software.[31]

4.2.2 | Molecular docking

Docking study was performed using DOCK6 software,[32] for the optimized ligand and complex structures against *C. albicans* protein enzyme (CYP51)[33] (available in the Protein Data Bank database: http://www.rcsb.org/pdb; PDB ID: 5V5Z). Docked conformations were analyzed by applying the flexible docking algorithm, where the most favorable conformations were those with the highest score based on docking energy. Docking performance was improved by using atomic charges calculated in the DFT optimization step.

Pre-docking structures were prepared using UCSF Chimera 1.14,[34] through the addition of hydrogens atoms and standard charges to the protein structure, and identifying the ligand atom type according to the MM force field. It had been used to screen the docking results and identify the substrate/active site interaction.

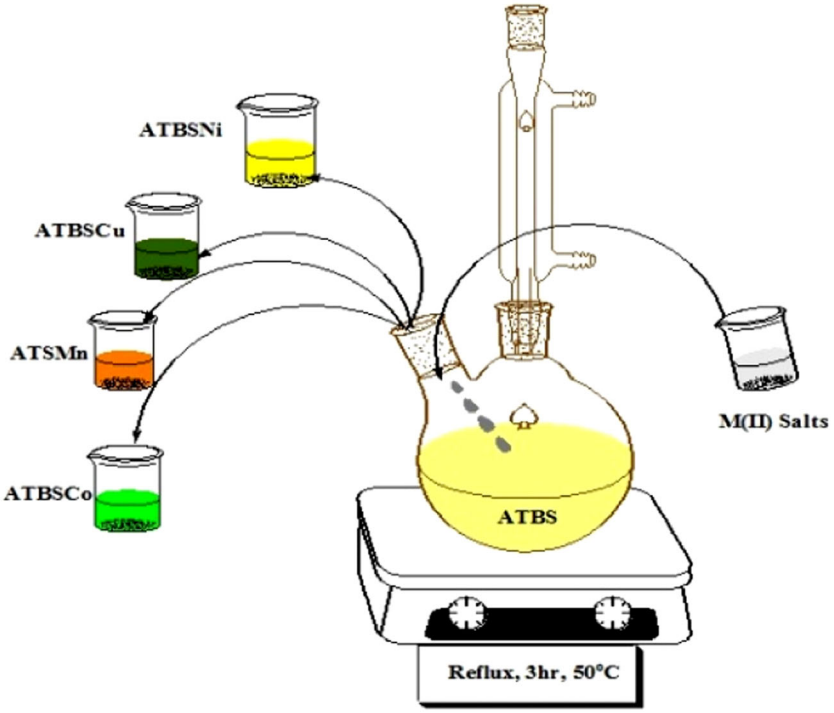

SCHEME 1 The synthesis of ATBS Schiff base complexes. ATBS, 4-bromo-2-(thiazole-2-yliminomethyl)phenol

To make docking more reliable, DFT atomic charges of the substrates were used; also, the maximum orientation of the substrate in the active pocket was increased to 10,000 steps and the favorable conformations were selected on the basis of the lowest energy score.[35]

4.3 | Biological assays

4.3.1 | Antimicrobial activity

Antibacterial evaluation

The novel Schiff base ligand and its complexes were tested for their antibacterial activity against the pathogenic Gram-negative bacterium *E. coli*, and two Gram-positive bacteria *B. subtilis* and *S. aureus*, by disc diffusion technique, which was carried out at two different concentrations 10 and 20 mg/ml of the tested compounds.[36] Agar nutrient was used as a medium and tetracycline as a standard. The stock solutions of the presented compounds were dissolved in DMSO. In a typical procedure, agar plates are inoculated with the selected pathogenic microorganisms. Then, filter paper discs (6 mm in diameter) containing the test solution at the desired concentration are placed on the agar surface. The Petri dishes were incubated at 37°C overnight. By the diffusion of the test solution, the microorganisms are affected and inhibited. The antibacterial activity is evaluated by measuring the inhibition zone diameter.

Antifungal evaluation

The in vitro antifungal evaluation of all synthesized compounds was screened against three types of fungi: *C. albicans*, *A. flavus*, and *T. rubrum* via the disc diffusion method. Estimation of the antifungal activity was carried out in the presence of DMSO as a solvent and a control, as it has no activity against the selected fungi. In such a method, fluconazole was used as a standard. The investigated compounds were poured in Petri plates with 5 mm diameter and 1 mm thickness. Two separate concentrations, 10 and 20 mg/ml, of the test compounds in DMSO were prepared. The fungal culture plates were processed with inoculation and incubation for 3 days at 37°C. The plates were observed after 36 h of the incubated period and the diameters of inhibition zones in millimeters were measured. The activity index was calculated using the following relation:

$$\%\ \text{Activity index} = \frac{\text{Inhibition zone of the tested compound (mm)}}{\text{Inhibition zone of standard (mm)}} \times 100. \quad (9)$$

4.3.2 | Anticancer activity

The colon carcinoma (HCT-116 cell line) and hepatocellular carcinoma (Hep-G2 cell line) cells were obtained from the National Cancer Institute, Cancer Biology Department, Pharmacology Department, Cairo University. The SRB is the technique used for estimation of the in vitro cytotoxicity of both Co(II) and Cu(II) and Mn(II) complexes.[37,38] In this method, 96-well plates (10^4 cells/well) were used for saving the cancer cells for 24 h before testing the effect of the prepared complexes to allow the attachment of the cells to the wall of the plate. Different concentrations of the two investigated complexes (0.00, 1.65, 3.125, 6.25, 12.50, 25.00, and 50.00 μM) were prepared in DMSO and added to the cancer cells. The plates were incubated for 48 h at 37°C, and then the cells were fixed, rinsed, and

stained with SRB stain. Acetic acid and Tris-EDTA buffer were used to wash the excess stain and treatment of the other attachement, and evaluation of IC_{50} was performed.

4.3.3 | Methodology of DNA binding studies

Electronic absorption spectra

CT-DNA was empolyed to probe the electronic spectral changes of the investigated complexes upon dissolving in Tris-HCl buffer (60 mM, pH 7.2). The spectral evaluation of DNA–buffer solution presented a UV absorption at 260 and 280 nm, which is equal to 1.8–1.9, indicating no protein contaminations in DNA.[39–41] Determination of DNA concentration was carried out by measuring the UV absorption at 260 nm, utilizing the molar absorption coefficient $\varepsilon_{260} = 6600\ M^{-1}\ cm^{-1}$. The prepared DNA stock solutions were kept at 4°C. The electronic absorption spectra of DNA measurements were carried out by maintaining the complex at a constant concentration, while varying the DNA concentration over a range of 30–150 μM. Preparation of DNA in the presented buffer was sufficient for removing the absorption of free CT-DNA, so the resulting spectra were due to the interaction of metal complex and DNA.[42] The binding constant (k_b) for the complex interaction with DNA was calculated from the resulting data using Equation (10), as shown in Table S8:

$$\frac{[DNA]}{(\varepsilon_a - \varepsilon_f)} = \frac{[DNA]}{(\varepsilon_b - \varepsilon_f)} + \frac{1}{k_b(\varepsilon_b - \varepsilon_f)}, \quad (10)$$

where [DNA] represents the concentration per nucleotide and $\mathcal{E}_a$ is the apparent coefficient that can be determined by calculating A_{obs}/[DNA]. Both $\mathcal{E}_f$ and $\mathcal{E}_b$ refer to the extinction coefficient of the free (unbound) and fully bounded complex, respectively. k_b was obtained by plotting [DNA]/($\mathcal{E}_a - \mathcal{E}_f$) versus [DNA], the slope equals 1/($\mathcal{E}_b - \mathcal{E}_f$) and the intercept 1/$k_b$ ($\mathcal{E}_b - \mathcal{E}_f$). Furthermore, the standard Gibbs free energy ΔG^0 for DNA binding was calculated from the following relation:

$$\Delta G^0 = -RT \ln k_b. \quad (11)$$

Viscosity measurements

The viscosity measurements were carried out on an Oswald microviscometer by fixing the concentration of DNA at 250 μM, whereas the concentration of the complex was varied over a range of 10–250 μM at constant temperature 25 ± 1°C, and the flow times were recorded for the different concentrations of the complexes. Bubbling nitrogen gas through the viscometer is necessary for good mixing of the solution. The mixture was left for 10 min at 37°C after each addition of the complex. The flow time was recorded with a digital stopwatch. The viscosity experiments were recorded in triplicate for each complex for obtaining the concurrent values. The obtained data are presented as $(\eta/\eta^o)^{1/3}$ versus the mole ratio [complex]/(DNA),[43] where η and η^o are the viscosity values of DNA in the presence and absence of the complex. The relative viscosity values of DNA in the presence and absence of the complex are calculated using the relation $\eta = (t - t^o)/t^o$, where t^o is the observed flow time of the DNA-containing solution and t is the flow time of the buffer alone. The relative viscosities of DNA are calculated from the relation (η/η^o).

Agarose gel electrophoresis

Agarose gel is an appropriate method for studying the extent of DNA binding with Schiff base complexes. Before the beginning of each experiment, the solutions of DNA were prepared by dissolving CT-DNA in redistilled water containing 0.1 M Tris-HCl buffer with adjustment of pH at 7.2. The preparation of the stock solution of each complex was done by dissolving 20 mg of the tested complex in 20 ml of DMF. The gel electrophoresis method was carried out by incubation of 25 μg/ml of the sample added to the isolated CT-DNA for 1 h at 37°C. The prepared samples were subjected to electrophoresis on the previously prepared 1% agarose gel in Tris/borate/EDTA (TBE) buffer containing 45 mM Tris, 45 mM boric acid, and 1 mM EDTA at pH 7.3. Then, 20 μl from the incubated mixture of both the complex and DNA was incubated for 30 min at 37°C. The incubated DNA and complex mixture was then loaded on the gel with 0.25% bromophenol blue dye in 1:1 ratio. The electrophoresis was undertaken in TBE at constant voltage (100 V) for 2 h, until the bromophenol dye reached up to 50% of the gel. After complete migration of DNA, the electric current was turned off and the gel was stained with 0.5 μg/ml of EB in water for 30–45 min at room temperature. Finally, it was visualized under UV light using a transilluminator and photographed with a Panasonic DMC-LZ5 Lumix digital camera.[44]

ACKNOWLEDGMENT

The authors acknowledge researchers supporting project number (RSP-2020/79), at King Saud University, Riyadh, Saudi Arabia, for funding this study.

CONFLICTS OF INTERESTS

The authors declare that there are no conflicts of interests.

ORCID

Mohamed Ismael https://orcid.org/0000-0002-3399-9813
Laila H. Abdel-Rahman https://orcid.org/0000-0001-7375-2885
Doaa Abou El-ezz https://orcid.org/0000-0002-8299-7259
Ayman Nafady https://orcid.org/0000-0003-1484-6894

REFERENCES

[1] A. N. M. Alaghaz, H. A. Bayoumi, *Int. J. Electrochem. Sci.* **2013**, *8*, 11860.
[2] B. Bhattacharya, D. K. Maity, P. Pachfule, E. Colacio, D. Ghoshal, *Inorg. Chem. Front.* **2014**, *1*, 414.
[3] P. G. Cozzi, *Chem. Soc. Rev.* **2014**, *33*(*7*), 410.
[4] N. G. Yernale, M. B. H. Mathada, *Bioinorg. Chem. Appl.* **2014**, *314963*, 1.
[5] H. M. A. El-Lateef, M. Ismael, I. M. A. Mohamed, *Corros. Rev.* **2015**, *33*(*1–2*), 77.

[6] L. H. Abdel-Rahman, R. M. El-Khatib, L. A. Nassr, A. M. Abu-Dief, M. Ismael, A. A. Seleem, *Spectrochim. Acta A* **2014**, *117*, 366.
[7] X. L. Zhang, H. X. Ouyang, Y. H. Ding, *Adv. Mater. Res.* **2012**, *396*, 2489.
[8] I. P. Ejidike, A. Peter, *Molecules* **2015**, *20*(*6*), 9788.
[9] M. Ismael, A. M. M. Abdel-Mawgoud, M. K. Rabia, A. Abdou, *Inorg. Chim. Acta* **2020**, *505*, 119443.
[10] A. A. Shanty, K. G. Raghu, P. V. Mohanan, *J. Mol. Struct.* **2019**, *1197*, 154.
[11] L. H. Abdel-Rahman, A. M. Abu-Dief, E. F. Newair, S. K. Hamdan, *J. Photochem. Photobiol., B* **2016**, *160*, 18.
[12] M. Nikoorazm, F. Ghorbani, A. Ghorbani-Choghamarani, Z. Erfani, *Phosphorus, Sulfur Silicon Relat. Elem.* **2018**, *193*(*9*), 552.
[13] M. S. More, P. G. Joshi, Y. K. Mishra, P. K. Khanna, *Mater. Today Chem.* **2019**, *14*, 100195.
[14] N. Raman, A. Selvan, *J. Mol. Struct.* **2011**, *985*, 173.
[15] L. H. Abdel-Rahman, M. S. S. Adam, A. M. Abu-Dief, H. Moustafa, M. T. Basha, A. S. Aboraia, B. S. Al-Farhan, H. E. Ahmed, *Appl. Organometal. Chem.* **2017**, *31*(*11*), e3750.
[16] L. H. Abdel-Rahman, A. A. Abdelhamid, A. M. Abu-Dief, M. R. Shehata, M. A. Bakheet, *J. Mol. Struct.* **2020**, *1200*, 127034.
[17] A. P. Mishra, K. J. Rajendra, *J. Saudi Chem. Soc.* **2014**, *18*(*6*), 814.
[18] T. R. Rao, P. Archana, *Synth. React. Inorg. Met-Org. Chem.* **2005**, *35*, 299.
[19] D. M. Loredana, A. Kriza, A. M. Musuc, *J. Therm. Anal. Calorim.* **2013**, *112*(*2*), 585.
[20] H. M. A. El-Lateef, A. M. Abu-Dief, M. A. Mohamed, *J. Mol. Struct.* **2017**, *1130*, 522.
[21] M. T. Basha, R. M. Alghanmi, M. R. Shehata, L. H. Abdel-Rahman, *J. Mol. Struct.* **2019**, *1183*, 298.
[22] M. Joseph, M. Kuriakose, M. R. P. Kurup, E. Suresh, A. Kishore, S. G. Bhat, *Polyhedron* **2006**, *25*, 61.
[23] Y. Dong, X. Liu, Y. An, M. Liu, J. Han, B. Sun, *Bioorg. Chem.* **2020**, *99*, 103749.
[24] A. M. Abu-Dief, L. H. Abdel-Rahman, M. R. Shehata, A. A. H. Abdel-Mawgoud, *J. Phy. Org. Chem.* **2019**, *32*(*12*), e4009.
[25] L. H. Abdel-Rahman, A. M. Abu-Dief, M. Ismael, M. A. Mohamed, N. A. Hashem, *J. Mol. Struct.* **2016**, *1103*, 2327.
[26] L. H. Abdel-Rahman, N. M. Ismail, M. Ismael, A. M. Abu-Dief, E. A. H. Ahmed, *J. Mol. Struct.* **2017**, *1134*, 851.
[27] M. S. Ray, A. Ghosh, R. Bhattacharya, G. Mukhopadhyay, M. G. B. Drew, J. Ribas, *Dalton Trans.* **2004**, *2*, 252.
[28] M. J. Frisch, G. W. Trucks, H. B. Schlegel, G. E. Scuseria, M. A. Robb, J. R. Cheeseman, J. A. Montgomery, Jr., T. Vreven, K. N. Kudin, J. C. Burant, J. M. Millam, S. S. Iyengar, J. Tomasi, V. Barone, B. Mennucci, M. Cossi, G. Scalmani, N. Rega, G. A. Petersson, H. Nakatsuji, M. Hada, M. Ehara, K. Toyota, R. Fukuda, J. Hasegawa, M. Ishida, T. Nakajima, Y. Honda, O. Kitao, H. Nakai, M. Klene, X. Li, J. E. Knox, H. P. Hratchian, J. B. Cross, V. Bakken, C. Adamo, J. Jaramillo, R. Gomperts, R. E. Stratmann, O. Yazyev, A. J. Austin, R. Cammi, C. Pomelli, J. W. Ochterski, P. Y. Ayala, K. Morokuma, G. A. Voth, P. Salvador, J. J. Dannenberg, V. G. Zakrzewski, S. Dapprich, A. D. Daniels, M. C. Strain, O. Farkas, D. K. Malick, A. D. Rabuck, K. Raghavachari, J. B. Foresman, J. V. Ortiz, Q. Cui, A. G. Baboul, S. Clifford, J. Cioslowski, B. B. Stefanov, G. Liu, A. Liashenko, P. Piskorz, I. Komaromi, R. L. Martin, D. J. Fox, T. Keith, M. A. Al-Laham, C. Y. Peng, A. Nanayakkara, M. Challacombe, P. M. W. Gill, B. Johnson, W. Chen, M. W. Wong, C. Gonzalez, J. A. Pople, *Gaussian 03, Revision C.01*, Gaussian Inc., Wallingford, CT **2004**.
[29] M. Khairy, M. Ismael, R. M. El-Khatib, M. Abdelnaeem, M. Khalaf, *Anal. Methods* **2016**, *8*, 4977.
[30] M. Ismael, A. Abdou, A.-M. Abdel-Mawgoud, *Z. Anorg. Allg. Chem.* **2018**, *644*, 1203.
[31] Nielsen, A. B., A. J. Holder., GaussView 3.0, Gaussian Inc., Pittsburgh, PA 2003.
[32] P. T. Lang, S. R. Brozell, S. Mukherjee, E. F. Pettersen, E. C. Meng, V. Thomas, R. C. Rizzo, D. A. Case, T. L. James, I. D. Kuntz, *RNA* **2009**, *15*, 1219.
[33] M. V. Keniya, M. Sabherwal, R. K. Wilson, A. A. Sagatova, J. D. A. Tyndall, B. C. Monk, *Antimicrob. Agents Chemother.* **2018**, *62*(*11*), e01134.
[34] E. F. Pettersen, T. D. Goddard, C. C. Huang, G. S. Couch, D. M. Greenblatt, E. C. Meng, T. E. Ferrin, *J. Comput. Chem.* **2004**, *1605*, 25.
[35] A. Khodairy, E. A. Ahmed, M. Ismael, K. M. Mohamed, S. A. Thabet, *J. Heterocycl. Chem.* **2019**, *56*, 1055.
[36] M. S. S. Adam, L. H. Abdel-Rahman, A. M. Abu-Dief, N. A. Hashem, *Inorg. Nano-Met. Chem.* **2020**, *50*(*3*), 136.
[37] L. H. Abdel-Rahman, Ahmed M. Abu-Dief., R. M. El-Khatib, S. M. Abdel-Fatah, *J. Photochem. Photobiol., B* **2016**, *162*, 298.
[38] S. S. Hindo, M. Frezza, D. Tomco, M. J. Heeg, L. Hryhorczuk, B. R. McGarvey, Q. P. Dou, C. N. Verani, *Eur. J. Med. Chem.* **2009**, *44*, 4353.
[39] L. H. Abdel-Rahman, M. S. S. Adam, A. M. Abu-Dief, H. Moustafa, M. T. Basha, A. S. Aboraia, B. S. Al-Farhan, H. E. Ahmed, *App. Organometal. Chem.* **2018**, *32*(*12*), e4527.
[40] L. H. Abdel-Rahman, R. M. El-Khatib, L. A. E. Nassr, Ahmed M. Abu-Dief, *J. Mol. Struct.* **2013**, *1040*, *9*.
[41] L. H. Abdel-Rahman, R. M. El-Khatib, L. A. E. Nassr, A. M. Abu-Dief, F. E.-D. Lashin, *Spectrochim. Acta A* **2013**, *111*, 266.
[42] M. Sirajuddin, N. Uddin, S. Ali, M. N. Tahir, *Spectrochim. Acta* **2013**, *116*, 111.
[43] L. H. Abdel Abdel-Rahman, Ahmed M. Abu-Dief., H. Moustafa, S. K. Hamdan, *Appl. Organometal. Chem.* **2017**, *31*, e3555.
[44] L. H. Abdel Abdel-Rahman, Ahmed M. Abu-Dief., R.M. El-Khatib., S. M. Abdel-Fatah, *Bioorg. Chem.* **2016**, *69*, 140.

SUPPORTING INFORMATION

Additional Supporting Information may be found online in the supporting information tab for this article.

How to cite this article: Ismael M, Abdel-Rahman LH, Abou El-ezz D, Ahmed EA-H, Nafady A. Synthesis, structural characterization, and biological studies of ATBS–M complexes (M(II) = Cu, Co, Ni, and Mn): Access for promising antibiotics and anticancer agents. *Arch Pharm.* 2020;e2000241. https://doi.org/10.1002/ardp.202000241